

## Novel Configurational-Bias Monte Carlo Method for Branched Molecules. Transferable Potentials for Phase Equilibria. 2. United-Atom Description of Branched Alkanes

Marcus G. Martin and J. Ilja Siepmann\*

Department of Chemistry and Department of Chemical Engineering and Materials Science, University of Minnesota, 207 Pleasant St. SE, Minneapolis, Minnesota 55455-0431

Received: December 14, 1998; In Final Form: March 17, 1999

A new generalization of the configurational-bias Monte Carlo method is presented which avoids the problems inherent in a Boltzmann rejection scheme for sequentially generating bond bending and torsional angles. The TraPPE-UA (transferable potentials for phase equilibria united-atom) force field is extended to include Lennard-Jones interaction parameters for methine and quaternary carbon groups by fitting to critical temperatures and saturated liquid densities of branched alkanes. Configurational-bias Monte Carlo simulations in the Gibbs ensemble were carried out to determine the vapor–liquid coexistence curves (VLCC) for six alkane isomers with four to eight carbons. Results are presented for two united-atom alkane force fields: PRF [Poncela, et al. *Mol. Phys.* **1997**, *91*, 189] and TraPPE-UA. Standard-state specific densities for the TraPPE-UA model were studied by simulations in the isobaric–isothermal ensemble. It is found that a single set of methyl, methylene, methine, and quaternary carbon parameters gives a reasonable description of the fluid phases of all alkanes with two or more carbon atoms. Whereas the size of the united atoms increases with increasing number of hydrogens for the PRF force field, it is demonstrated here that the opposite trend yields a better fit to the experimental VLCC data. The TraPPE-UA force field underpredicts the magnitude of the experimental second virial coefficients, while PRF gives good second virial coefficients but does not perform satisfactorily for the VLCC. As is also seen for the normal alkanes, the TraPPE-UA force field shows small, systematic deviations from the experimental saturated vapor pressures and densities for all molecules studied, and it slightly overpredicts the critical temperatures of the larger branched alkanes.

### 1. Introduction

Alkane isomers provide an excellent example of how molecular architecture affects macroscopic physical properties. Branched alkanes generally are better lubricants and fuels and have lower critical temperatures and boiling points than the corresponding linear isomers. These interesting properties, along with a wealth of experimental data, make the alkanes very attractive as a starting point for developing a transferable molecular force field. One approach for describing isomeric alkanes is to have two types of interaction sites centered on the atomic positions, one for the carbons and one for the hydrogens.<sup>1</sup> Another approach is to consider four different pseudo-atoms, namely methyl, methylene, methine, and quaternary carbons, and to place these united atoms either at the carbon centers<sup>2</sup> or displaced toward the hydrogens.<sup>3</sup> In this paper, we will only consider united atoms centered on carbon atoms in order to determine what level of accuracy can be obtained from this relatively simple (and less expensive) description of the alkanes.

The motivation for this work was to find an optimized set of united-atom Lennard-Jones (LJ) methine (CH) and quaternary carbon (C) parameters for branched alkanes while retaining methyl and methylene groups previously derived for the *n*-alkanes.<sup>4</sup> Molecular simulations for two sets of alkane parameters (force fields) are described in this paper. The first model tested was the united-atom force field of Poncela, Rubio, and Freire<sup>5</sup> (PRF) which was parameterized to yield accurate second virial coefficients for linear and branched alkanes. While

fitting their model, they enforced the condition that both the well depth and diameter of the Lennard-Jones pseudo-atoms increase with increasing number of hydrogens.

The second molecular model presented is the transferable potentials for phase equilibria united-atom (TraPPE-UA) force field. Unlike the PRF force field, the TraPPE-UA force field is based upon calculations of VLCC. The methyl and methylene group LJ parameters were previously obtained from simulations of *n*-alkanes<sup>4</sup> and were retained for the branched alkanes. The methine parameters were fitted to give accurate VLCC for isobutane (2-methylpropane), and the quaternary carbon parameters were fitted to the VLCC of neopentane (2,2-dimethylpropane). This fitting strategy results in a well depth that increases, and a diameter that decreases, with increasing number of hydrogens. Unlike some recent similar force fields,<sup>6,7</sup> the TraPPE-UA force field parameters for a given pseudo-atom do not depend upon its neighboring pseudo-atoms. The TraPPE-UA force field describes the alkanes with only four types of pseudo-atoms, which allows for maximum simplicity and transferability. While it could be argued that the parameters of pseudo-atoms should depend upon their nearest neighbors, such a force field for the alkanes would have 69 different types of pseudo-atoms. Most likely, such a force field could reproduce the available VLCC data quite well, but it would be an enormous task to optimize all of these parameters. See the first paper in this series<sup>4</sup> for a more complete description of the goals and constraints of the TraPPE-UA force field.

In the course of performing the simulations it became evident that the configurational-bias Monte Carlo (CBMC) procedure

\* Corresponding author: E-mail: siepmann@chem.umn.edu.

**TABLE 1: Comparison of the Lennard-Jones Parameters for the PRF<sup>5</sup> and TraPPE-UA Force Fields**

pseudo-atom	PRF		TraPPE-UA	
	$\epsilon/k_B$ [K]	$\sigma$ [Å]	$\epsilon/k_B$ [K]	$\sigma$ [Å]
CH <sub>4</sub>	140	4.10	148	3.73
CH <sub>3</sub>	96	4.02	98	3.75
CH <sub>2</sub>	57	3.72	46	3.95
CH	36	3.36	10	4.68
C	9	2.44	0.5	6.4

used previously by several research groups<sup>7–10</sup> (including our own) for growing branched molecules is not only very inefficient (such that a CBMC move for a branched molecule is several times more expensive than a CBMC move for a linear molecule of the same size) but also sometimes results in incorrect distributions of bond bending and torsional angles. We present a new CBMC method that is computationally efficient and generates the proper distribution of angles for any branched molecular architecture.

This paper is organized as follows. First, we briefly describe the two alkane force fields and the simulation methods used. Then, we present the new CBMC algorithm. Finally, we report and discuss single-component data obtained for the force fields, including VLCC, critical points, boiling points, standard specific densities, second virial coefficients, and conformational statistics.

## 2. Models

The TraPPE-UA and PRF alkane models are based on the united-atom description. In both cases, the nonbonded interactions between pseudo-atoms which are separated by more than three bonds, or belong to different molecules, are described solely by pairwise-additive Lennard-Jones 12-6 potentials

$$u(r_{ij}) = 4\epsilon_{ij} \left[ \left( \frac{\sigma_{ij}}{r_{ij}} \right)^{12} - \left( \frac{\sigma_{ij}}{r_{ij}} \right)^6 \right] \quad (1)$$

where  $r_{ij}$ ,  $\epsilon_{ij}$ , and  $\sigma_{ij}$  are the separation, LJ well depth, and LJ size, respectively, for the pair of atoms  $i$  and  $j$ . The LJ parameters for interactions between like pseudo-atoms are listed in Table 1. Unlike interactions are computed using standard Lorentz–Berthelot combining rules<sup>11,12</sup>

$$\begin{aligned} \sigma_{ij} &= \frac{1}{2}(\sigma_{ii} + \sigma_{jj}) \\ \epsilon_{ij} &= \sqrt{\epsilon_{ii}\epsilon_{jj}} \end{aligned} \quad (2)$$

Pseudo-atoms are connected by fixed bond lengths (1.54 Å for all bonds in the TraPPE-UA force field). Bond angle bending is governed by a harmonic potential

$$u_{\text{bend}} = \frac{1}{2}k_{\theta}(\theta - \theta_0)^2 \quad (3)$$

with the force constant proposed by van der Ploeg and Berendsen,<sup>13</sup> and the motion of the dihedral angles  $\phi$  is governed by a united-atom torsional potential of the familiar OPLS form<sup>14</sup>

$$u_{\text{tors}} = c_0 + c_1[1 + \cos \phi] + c_2[1 - \cos(2\phi)] + c_3[1 + \cos(3\phi)] \quad (4)$$

**TABLE 2: Bonded Parameters for the TraPPE-UA Force Field**

stretch	$r_0$ [Å]			
CH <sub>x</sub> –CH <sub>y</sub>	1.54			
bend	$\theta_0$	$k_{\theta}/k_B$ [K]		
CH <sub>x</sub> –(CH <sub>2</sub> )–CH <sub>y</sub>	114	62 500		
CH <sub>x</sub> –(CH)–CH <sub>y</sub>	112	62 500		
CH <sub>x</sub> –(C)–CH <sub>y</sub>	109.47	62 500		
torsion	$c_0/k_B$ [K]	$c_1/k_B$ [K]	$c_2/k_B$ [K]	$c_3/k_B$ [K]
CH <sub>x</sub> –(CH <sub>2</sub> )–(CH <sub>2</sub> )–CH <sub>y</sub>	0	335.03	–68.19	791.32
CH <sub>x</sub> –(CH <sub>2</sub> )–(CH)–CH <sub>y</sub>	–251.06	428.73	–111.85	441.27
CH <sub>x</sub> –(CH <sub>2</sub> )–(C)–CH <sub>y</sub>	0	0	0	461.29
CH <sub>x</sub> –(CH)–(CH)–CH <sub>y</sub>	–251.06	428.73	–111.85	441.27

where the appropriate constants<sup>15</sup> for the TraPPE-UA force field are listed in Table 2. These bonded parameters were also used for the PRF force field, but the C–C bond lengths were set to the PRF values<sup>5</sup> of 1.55 Å for neopentane and 1.53 Å for isobutane.

## 3. Simulation and Analysis Methods

**A. Vapor–Liquid Coexistence Curves.** A combination<sup>16,17</sup> of the Gibbs ensemble Monte Carlo (GEMC) technique<sup>18–20</sup> and the configurational-bias Monte Carlo (CBMC) method<sup>21–24</sup> was used to determine the VLCC. The simulation details are identical to those given in our previous paper,<sup>4</sup> except for the CBMC method.

The CBMC method previously used by us<sup>7–9</sup> and by others<sup>10,25</sup> for branched alkanes generates conformations according to the probability

$$P_{\text{gen}} = \prod_{n=1}^{n_{\text{step}}} \left[ \frac{\exp(-\beta u_{\text{LJ}}(i))}{W(n)} \right] \exp(-\beta u_{\text{tors}}(i)) \exp(-\beta u_{\text{bend}}(i)) \quad (5)$$

$$W(n) = \sum_{i=1}^{n_{\text{choice}}} \exp(-\beta u_{\text{LJ}}(i)) \quad (6)$$

where  $n$  is the growth step,  $n_{\text{step}}$  is the total number of growth steps,  $i$  is a particular trial,  $n_{\text{choice}}$  is the number of trials for which the Lennard-Jones interactions are computed,  $\beta = (k_B T)^{-1}$  is the inverse temperature, and  $W(n)$  is the Rosenbluth weight for growth step  $n$ . A move is accepted with probability

$$P_{\text{acc}} = \text{Min} \left[ 1, \frac{\prod_{n=1}^{n_{\text{step}}} W(n)_{\text{new}}}{\prod_{n=1}^{n_{\text{step}}} W(n)_{\text{old}}} \right] \quad (7)$$

where the calculation of the Rosenbluth weights of the old configuration uses the original conformation to compute the Boltzmann weight for  $i = 1$ . This method requires the generation of bond vectors which sample the proper distribution of bond bending and torsional angles for use as trial sites in the Lennard-Jones biased selection. This is usually accomplished by choosing a vector uniformly on a unit sphere, computing its bond bending and torsional energy, and accepting the vector if a random

number uniform on (0,1) is less than the Boltzmann weight. This Boltzmann rejection process is repeated until  $n_{\text{choice}}$  vectors are accepted.

Vlugt and Smit have recently shown that using the Boltzmann rejection scheme to sequentially generate bond bending angles does not result in the correct distribution of angles for branched molecules.<sup>26</sup> This problem can be avoided for certain branched molecules and force fields by either performing an additional Monte Carlo simulation to determine the bond angles<sup>26</sup> or by growing all atoms from a branch point simultaneously.<sup>25</sup> Unfortunately, these methods still fail to generate the proper distribution when there are multiple torsional angles that share the same two central atoms because the bond bending and torsional angle distributions are no longer independent. In that case, all of the atoms connected to those central atoms must be generated simultaneously in order to get the correct distribution. This is disastrous for a molecule like 2,3-dimethylbutane, as the conformation of the entire molecule must be generated in a single step in order to obtain the correct distribution.

A straight-forward way to avoid this problem is to include the bond bending and torsional energies with the Lennard-Jones energy when performing the biased growth of the molecule.

$$P_{\text{gen}} = \prod_{n=1}^{n_{\text{step}}} \left[ \frac{\exp(-\beta u_{\text{LJ}}(i)) \exp(-\beta u_{\text{tors}}(i)) \exp(-\beta u_{\text{bend}}(i))}{W(n)} \right] \quad (8)$$

$$W(n) = \sum_{i=1}^{n_{\text{choice}}} \exp(-\beta[u_{\text{LJ}}(i) + u_{\text{tors}}(i) + u_{\text{bend}}(i)]) \quad (9)$$

The regrowth is accepted with probability

$$P_{\text{acc}} = \text{Min} \left[ 1, \frac{\prod_{n=1}^{n_{\text{step}}} W(n)_{\text{new}}}{\prod_{n=1}^{n_{\text{step}}} W(n)_{\text{old}}} \right] \quad (10)$$

In fact, this approach is essentially identical to the method presented by de Pablo and co-workers for linear alkanes with fixed bond angles.<sup>24</sup> While this method does always sample the correct distribution, it is computationally extremely inefficient for molecules with strong intramolecular potentials (such as bond bending) because it takes a relatively large number of trial sites to find a few that have reasonable bond angles. This means that the more expensive Lennard-Jones energy must be calculated for a large number of trial sites that have no significant probability of being selected during the growth because the large positive bond bending energy creates an extremely small Boltzmann weight. One could instead use a nonsequential Boltzmann rejection to determine the bond angles and then utilize a biased selection similar to eqs 8–10, but without the  $u_{\text{bend}}$  term. Macedonia and Maginn have proposed such a method, except they eliminate the computational burden of the Boltzmann rejection step by performing a presimulation to tabulate sets of bond angles for use during CBMC moves.<sup>27</sup>

It is also possible to decouple the selection of the different energies in a manner similar in spirit to multiple time step integrators in molecular dynamics.<sup>28</sup> In this case, the probability

to generate a given configuration and the corresponding Rosenbluth weights are given by

$$P_{\text{gen}} = \prod_{n=1}^{n_{\text{step}}} \left[ \frac{\exp(-\beta u_{\text{LJ}}(i))}{W_{\text{L}}(n)} \right] \left[ \frac{\exp(-\beta u_{\text{tors}}(j))}{W_{\text{T}}(n)} \right] \left[ \frac{\exp(-\beta u_{\text{bend}}(k))}{W_{\text{B}}(n)} \right] \quad (11)$$

$$W_{\text{L}}(n) = \sum_{i=1}^{n_{\text{chLJ}}} \exp(-\beta u_{\text{LJ}}(i)) \quad (12)$$

$$W_{\text{T}}(n) = \sum_{j=1}^{n_{\text{chtor}}} \exp(-\beta u_{\text{tors}}(j)) \quad (13)$$

$$W_{\text{B}}(n) = \sum_{k=1}^{n_{\text{chbend}}} \exp(-\beta u_{\text{bend}}(k)) \quad (14)$$

where  $n_{\text{chLJ}}$ ,  $n_{\text{chtor}}$ , and  $n_{\text{chbend}}$  are the number of trial sites for the Lennard-Jones, torsional, and bond bending interactions, respectively. The move is accepted with probability

$$P_{\text{acc}} = \text{Min} \left[ 1, \frac{\prod_{n=1}^{n_{\text{step}}} W_{\text{L}}(n)_{\text{new}} W_{\text{T}}(n)_{\text{new}} W_{\text{B}}(n)_{\text{new}}}{\prod_{n=1}^{n_{\text{step}}} W_{\text{L}}(n)_{\text{old}} W_{\text{T}}(n)_{\text{old}} W_{\text{B}}(n)_{\text{old}}} \right] \quad (15)$$

This decoupled selection has the advantage that a large number of trial sites can be chosen for the less expensive bond angle selection without increasing the cost of performing the other biased selections. Once the bond angle distribution has been chosen in a biased fashion, it is used as an input for the subsequent biased selections of the torsional and Lennard-Jones interactions. When calculating the old Rosenbluth weights, the original conformation is used to compute the Boltzmann factor when  $i = 1$ ,  $j = 1$ , or  $k = 1$ , and this original conformation is selected for use in the subsequent selections. The main drawback of this method is that, once the torsional angles have been chosen in a biased fashion, there is only one possible trial site available to the Lennard-Jones selection ( $n_{\text{chLJ}} = 1$ ).

The obvious way around the problem with the torsional selection is to group the torsional and Lennard-Jones energies together into a single biased step. However, this is inefficient for the same reason as was the case with the bond bending potential. Another way to approach the problem is to couple the biased selections so that each biased selection sends multiple possible conformations to the next selection step. In this case, we obtain

$$P_{\text{gen}} = \prod_{n=1}^{n_{\text{step}}} \left[ \frac{\exp(-\beta u_{\text{LJ}}(i)) W_{\text{T}}(i)}{W_{\text{L}}(n)} \right] \left[ \frac{\exp(-\beta u_{\text{tors}}(j)) W_{\text{B}}(j)}{W_{\text{T}}(i)} \right] \left[ \frac{\exp(-\beta u_{\text{bend}}(k))}{W_{\text{B}}(j)} \right] \quad (16)$$

$$W_{\text{L}}(n) = \sum_{i=1}^{n_{\text{chLJ}}} \exp(-\beta u_{\text{LJ}}(i)) W_{\text{T}}(i) \quad (17)$$

$$W_T(i) = \sum_{j=1}^{n_{\text{chtor}}} \exp(-\beta u_{\text{tors}}(j)) W_B(j) \quad (18)$$

$$W_B(j) = \sum_{k=1}^{n_{\text{chbend}}} \exp(-\beta u_{\text{bend}}(k)) \quad (19)$$

$$P_{\text{acc}} = \text{Min} \left[ 1, \frac{\prod_{n=1}^{n_{\text{step}}} W_L(n)_{\text{new}}}{\prod_{n=1}^{n_{\text{step}}} W_L(n)_{\text{old}}} \right] \quad (20)$$

This coupled biased growth now performs a separate torsional bias selection for each of the  $n_{\text{chLJ}}$  trial steps of the Lennard-Jones biased selection. During the old conformation regrowth, the original conformation is used only when  $i = j = k = 1$ . The disadvantage of coupling all of the energy types is that  $n_{\text{chLJ}}$   $n_{\text{chtor}}$   $n_{\text{chbend}}$  trial vectors must be generated for the bond angle bias selection.

A combination of the coupled and decoupled biased selections allows a great deal of flexibility when designing a CBMC scheme for a molecule. The specific implementation of CBMC used in this work performs a coupled biased selection for the Lennard-Jones and torsional selection steps, while splitting the bond bending energy into several decoupled biased selections. The details of this method are given in the Appendix. These new CBMC methods are also applicable to force fields which contain a greater number of terms than those considered in this work. For example, bond stretching could be added as another decoupled selection, and crossterms between bond stretches, bond angles, and torsions could be added into the selection which occurs later in the method (i.e., bending–torsion interactions computed in the torsional selection).

The Gibbs ensemble simulations were carried out for system sizes of 400 molecules. The total volume of the two simulation boxes was adjusted so that the liquid phase contained approximately 250 molecules and the vapor phase contained approximately 150 molecules. Moves were selected at random with a fixed probability where the fraction of CBMC-exchange moves was manually adjusted to obtain roughly 1 accepted molecule exchange per 10 cycles, the fraction of volume moves was 0.001, and the remainder of the moves were equally divided between translation of the center of mass (COM), rotation about the COM, and configurational-bias regrowths. The maximum translational, rotational, and volume displacements were adjusted automatically in order to yield 50% acceptance rates. Computational efficiency was improved by utilizing a biased insertion with 10 trial sites for the first pseudo-atom in a CBMC-exchange,<sup>29,30</sup> an additional COM-based cutoff which avoids computing unneeded distances,<sup>4</sup> and a short cutoff ( $r_{\text{CBMC}} = 5$  Å) for use during CBMC moves, which is then corrected to the full potential ( $r_{\text{cut}} = 14$  Å) with tail corrections in the acceptance rule.<sup>9</sup> Simulations were equilibrated for at least 25000 MC cycles during which the chemical potential, the pressure, and the difference in the number of molecule exchanges was monitored. The production periods consisted of 25000 MC cycles. Standard deviations of the ensemble averages were computed by breaking the production runs into five blocks.

It is interesting to compare the Gibbs ensemble simulation time for branched molecules with that for a linear molecule that contains the same number of Lennard-Jones sites. For systems of 2,5-dimethylhexane, 3,4-dimethylhexane, and *n*-octane, 1000

MC cycles, performed at 440 K, take approximately 230, 260, and 190 min of CPU time on an Intel Pentium II (@300 MHz). Considering that 3,4-dimethylhexane has a 5% higher liquid density than *n*-octane at these conditions and that it has more bond bends (10:6) and torsions (8:5), it is clear that the cost of the coupled–decoupled CBMC algorithm is rather insensitive to molecular architecture.

The critical properties are extrapolated from weighted linear fits of the subcritical simulation data to the density scaling law<sup>31</sup> for the critical temperature  $T_c$

$$\rho_{\text{liq}} - \rho_{\text{vap}} = B(T - T_c)^\beta \quad (21)$$

to the law of rectilinear diameters<sup>32</sup> for the critical density  $\rho_c$

$$\frac{1}{2}(\rho_{\text{liq}} - \rho_{\text{vap}}) = \rho_c + A(T - T_c) \quad (22)$$

and the Clausius–Clapeyron equation<sup>33</sup> for the critical pressure  $p_c$

$$\ln p = C + \frac{C'}{T} \quad (23)$$

where  $\rho_{\text{liq}}$  and  $\rho_{\text{vap}}$  are the saturated liquid and vapor densities;  $T$  and  $p$  are the temperature and pressure (obtained from the molecular virial<sup>34</sup>);  $A$ ,  $B$ ,  $C$ , and  $C'$  are constants, and  $\beta = 0.32$  is the critical exponent. The normal boiling temperature  $T_b$  is also estimated from eq 23. No finite-size or cross-over corrections were considered for the determination of the critical points. We have previously shown that these corrections are smaller than the statistical noise for the system sizes considered here.<sup>4</sup>

**B. Specific Densities.** Simulations in the isobaric–isothermal ensemble<sup>35</sup> were used to determine the specific densities of 2,3-dimethylbutane, 2,5-dimethylhexane, and 3,4-dimethylhexane at 298 K and 1 atm. Four types of moves were selected randomly, with a fixed probability of performing a volume move of 0.005, and the remainder equally distributed between CBMC, translation and rotation. The simulations were carried out for 250 molecules. The isobaric–isothermal ensemble simulations consisted of at least 10000 MC cycles for equilibration and 10000 MC cycles for production.

**C. Second Virial Coefficients.** The second virial coefficient,  $B(T)$ , of a fully flexible molecule is given by<sup>36,37</sup>

$$B(T) = -2\pi \int [\langle \exp[-U_{\text{inter}}(r_{12})/k_B T] \rangle_{\alpha_1, \alpha_2} - 1] r_{12}^2 dr_{12} \quad (24)$$

where  $U_{\text{inter}}$  and  $r_{12}$  are the intermolecular interaction energy and the distance between the COM of molecules 1 and 2 and  $\langle \dots \rangle_{\alpha_1, \alpha_2}$  denotes the canonical ensemble average sampled over conformations of molecules 1 and 2 which are Boltzmann weighted solely on their intramolecular energies. We evaluate this average by utilizing two simulation boxes, each containing a single chain which samples conformational space via rotational and CBMC moves. After every 10 Monte Carlo cycles, the intermolecular energy for the current two chain conformations is evaluated for COM separations from 0 to 500 Å with a 0.05 Å step size. Once the ensemble average has been computed, the second virial coefficient is determined via numerical integration using the trapezoid rule.<sup>38</sup> Averages were computed from four separate runs of 10000 cycles.



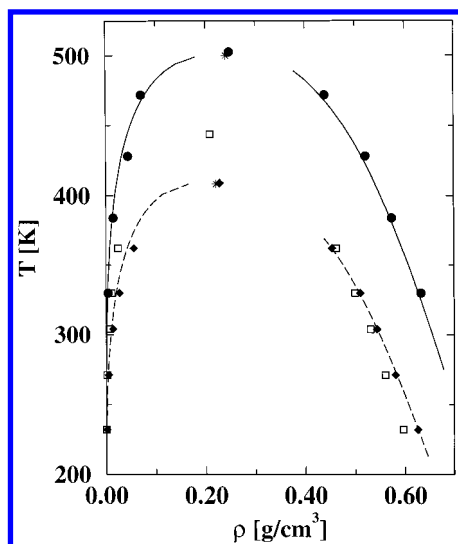


**Figure 1.** Vapor-liquid coexistence curves for isobutane (2-methylpropane) and 2,3-di-methylbutane. Experimental coexistence data and critical points<sup>41</sup> are shown as long dashed lines (isobutane), solid lines (2,3-dimethylbutane), and stars. Simulated coexistence densities and extrapolated critical points are shown for TraPPE-UA isobutane (filled diamonds), PRF isobutane (open squares), and TraPPE-UA 2,3-dimethylbutane (filled circles).

**D. Chain Conformations.** We performed some single-molecule calculations with a hit-and-miss integration program that creates individual molecule conformations from scratch by connecting  $n$  random vectors (where  $n$  is the number of bonds in that molecule). Properties are then calculated by simple Boltzmann averaging using the total energy (the sum of bond bending, torsional, and intramolecular Lennard-Jones interactions). This allows us to compare the angle and torsional distributions generated via our CBMC simulations with an independent, nonbiased generation of the same quantities.

#### 4. Results and Discussion

**A. Vapor-Liquid Coexistence Curves.** The goal for the fitting of the TraPPE-UA force field parameters was to give agreement with the experimental critical properties and coexistence densities to within the statistical accuracy of the simulations. As was discussed in the first paper in this series,<sup>4</sup> this goal appears to be unattainable for a united-atom 12-6 Lennard-Jones representation.<sup>39</sup> Instead, we parameterize in order to reproduce the experimental saturated liquid densities and critical temperatures. Following the philosophy that there should only be one set of LJ parameters for each type of carbon center in the alkanes, we determined the parameters for methine (CH) and quaternary carbon (C) from simulations of isobutane (2-methylpropane) and neopentane (2,2-dimethylpropane) using the methyl group parameters generated in previous work.

The VLCC for isobutane and neopentane were calculated for both the TraPPE-UA and PRF force fields as shown in Figures 1 and 2 (see also ref 40). The agreement of the TraPPE-UA results with experiment<sup>41</sup> is good for the coexistence liquid densities and the critical temperature. As seen also for the normal alkanes, even though the TraPPE-UA force field gives good liquid densities, it yields vapor densities that are consistently higher than experiment and boiling points which are too low (see Figure 3). In contrast, the PRF force field produces critical temperatures that are slightly too high and liquid densities which are too low. The critical pressures and boiling points were calculated using the Clausius-Clapeyron equation, and these

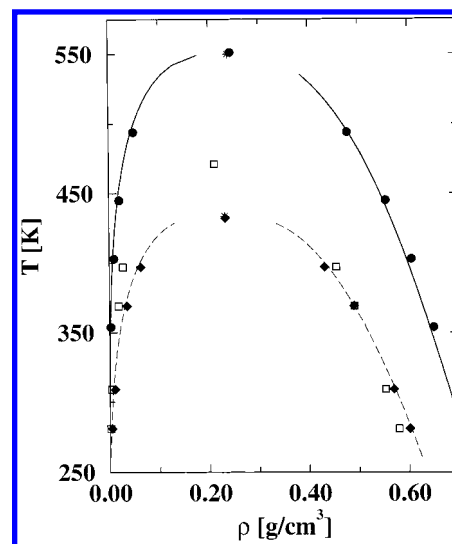


**Figure 2.** Vapor-liquid coexistence curves for neopentane (2,2-dimethylpropane) and 2,2-dimethylhexane. Experimental coexistence data and critical points<sup>41</sup> are shown as long dashed lines (neopentane), solid lines (2,2-dimethylhexane), and stars. Simulated coexistence densities and extrapolated critical points are shown for TraPPE-UA neopentane (filled diamonds), PRF neopentane (open squares), and TraPPE-UA 2,2-dimethylhexane (filled circles).

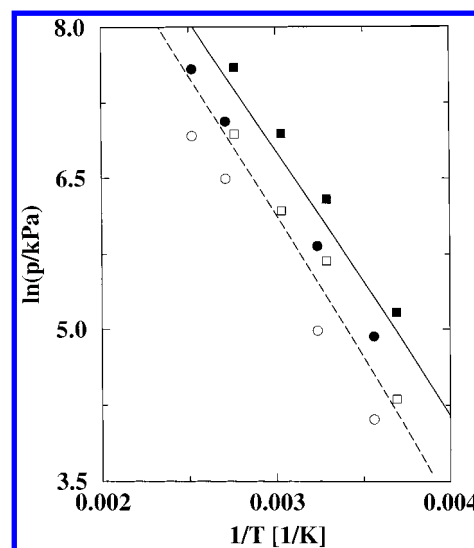


**Figure 3.** Clausius-Clapeyron plots of the saturated vapor pressures versus the inverse temperature. The experimental data<sup>41</sup> are shown for isobutane (solid line) and neopentane (long dashed line). Simulation data are shown for TraPPE-UA isobutane (filled squares), TraPPE-UA neopentane (filled circles), PRF isobutane (open squares), and PRF neopentane (open circles).

quantities are listed along with the other critical properties in Table 3.

The VLCCs for 2,3-dimethylbutane and 2,2-dimethylhexane reveal some of the limitations of the TraPPE-UA force field. The coexistence liquid densities are too high for both of these molecules. Thus, these two molecules require larger  $\sigma$  values in order to decrease the liquid densities. However, the current  $\sigma$  values already give liquid densities that are slightly too low for neopentane and isobutane, so increasing  $\sigma$  further will worsen the agreement for the smaller molecules. Thus, we are unable to find a single set of  $\sigma$  and  $\epsilon$  parameters that give perfect agreement with the liquid densities for a range of branched alkanes. In addition, the quaternary carbon  $\sigma$  parameter is unexpectedly large compared to the size of a methyl group, with a value of 6.4 Å. Clearly, some of the effect of crowding methyl

TABLE 3: Normal Boiling Points and Critical Properties Obtained from the Simulations<sup>a</sup>

alkane	force field/exptl	$T_b$ [K]	$T_c$ [K]	$\rho_c$ [g/mL]	$p_c$ [MPa]	$Z_c$
2-methylpropane (isobutane)	TraPPE-UA	252.6 <sub>12</sub>	408.9 <sub>23</sub>	0.228 <sub>3</sub>	4.4 <sub>9</sub>	0.33 <sub>7</sub>
	PRF	276.5 <sub>16</sub>	443.6 <sub>24</sub>	0.208 <sub>3</sub>	4.2 <sub>11</sub>	0.31 <sub>8</sub>
	exptl	261.4	408.1	0.221	3.6	0.283
2,2-dimethylpropane (neopentane)	TraPPE-UA	270.6 <sub>14</sub>	432.3 <sub>22</sub>	0.233 <sub>4</sub>	3.3 <sub>7</sub>	0.29 <sub>6</sub>
	PRF	296.4 <sub>11</sub>	471 <sub>4</sub>	0.221 <sub>5</sub>	3.3 <sub>8</sub>	0.29 <sub>7</sub>
	exptl	282.7	433.8	0.232	3.2	0.276
2,3-dimethylbutane	TraPPE-UA	320 <sub>4</sub>	503 <sub>3</sub>	0.248 <sub>3</sub>	3.8 <sub>17</sub>	0.32 <sub>14</sub>
	exptl	331.1	500.0	0.241	3.1	0.269
2,2-dimethylhexane	TraPPE-UA	368.6 <sub>15</sub>	551 <sub>5</sub>	0.244 <sub>6</sub>	2.9 <sub>8</sub>	0.30 <sub>8</sub>
	exptl	380.0	549.9	0.239	2.5	0.264
2,5-dimethylhexane	TraPPE-UA	375 <sub>1</sub>	559 <sub>3</sub>	0.238 <sub>4</sub>	2.7 <sub>5</sub>	0.28 <sub>5</sub>
	exptl	382.3	550.1	0.237	2.5	0.262
3,4-dimethylhexane	TraPPE-UA	382 <sub>2</sub>	584 <sub>3</sub>	0.247 <sub>3</sub>	3.0 <sub>5</sub>	0.28 <sub>5</sub>
	exptl	390.9	568.9	0.245	2.7	0.265

<sup>a</sup> Subscripts show the standard deviation in the final digit. The experimental boiling and critical points are taken from Smith and Srivastava.<sup>41</sup>

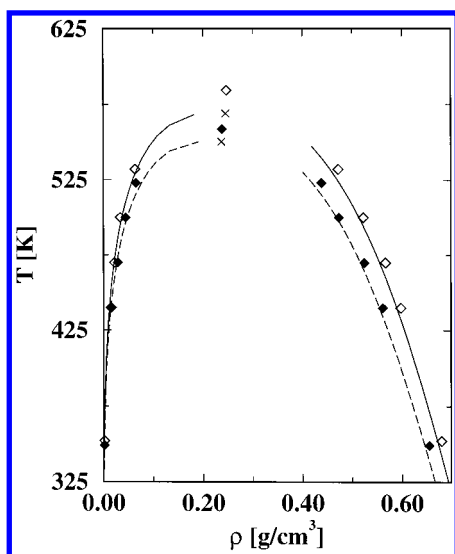


**Figure 4.** Vapor–liquid coexistence curves for 2,5-dimethylhexane and 3,4-dimethylhexane. Experimental coexistence data and critical points<sup>41</sup> are shown as long dashed lines (2,5-dimethylhexane), solid lines (3,4-dimethylhexane), and crosses. Simulated coexistence densities and extrapolated critical points for the TraPPE-UA force field are shown as filled diamonds (2,5-dimethylhexane) and open diamonds (3,4-dimethylhexane).

groups together around a quaternary carbon is being taken into account in the quaternary carbon parameters.

Despite these limitations, the TraPPE-UA force field has the ability to distinguish isomers that are composed of the same united-atom sites. The experimental critical temperature of 3,4-dimethylhexane is 19 K higher than that of 2,5-dimethylhexane and their saturated liquid densities differ by approximately 0.04 g/mL even though the compositions of both are identical with four methyl groups, two methylene groups, and two methine groups. The VLCCs of these two molecules, shown in Figure 4, demonstrate that TraPPE-UA produces the proper ordering of critical temperatures and liquid densities, although both are too high and the 25 K difference in  $T_c$  is larger than the experimentally observed value.

The trend of increasing  $\sigma$  with decreasing number of hydrogens that resulted from the fitting strategy for the TraPPE-UA model is opposite of the trend in the PRF model. Poncela et al. argue that under the assumption of additive hard-sphere volumes for individual carbon and hydrogen atoms, one should expect  $\sigma$  to be a linear function of the number of hydrogens.<sup>5</sup> This additive volume assumption was enforced during the fit of the PRF model. Figure 5 shows the vapor–liquid coexistence

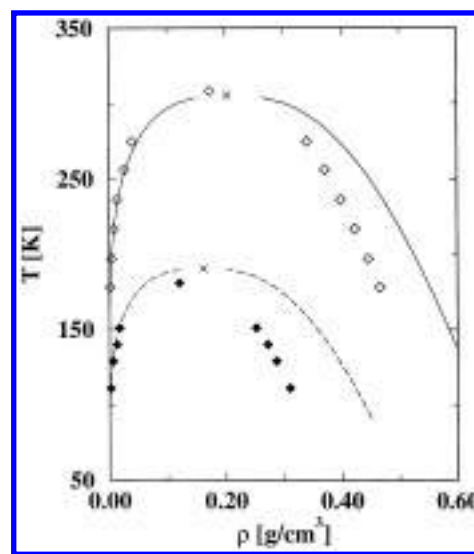


**Figure 5.** Vapor–liquid coexistence curves for methane and ethane. Experimental coexistence data and critical points<sup>41</sup> are shown as long dashed lines (methane), solid lines (ethane), and crosses. Simulated coexistence densities and extrapolated critical points for the PRF force field are shown as filled diamonds (methane) and open diamonds (ethane).

curves for methane and ethane calculated for the PRF model. While the saturated vapor densities and critical temperatures are quite well described, the saturated liquid densities are much lower than experiment. In particular, the relative deviations in the liquid densities are substantially larger for methane than for ethane. This is a clear indication that the ordering of  $\sigma$  values inferred from the additive volume assumption does not describe the physical reality well.

In contrast, the TraPPE-UA force field yields rather satisfactory liquid densities for methane, ethane, the larger linear alkanes and the branched alkanes. Using the additive volume assumption, one might infer that hydrogens contribute a negative amount of volume to the TraPPE-UA pseudo-atoms. However, the pseudo-atoms in alkanes overlap not only with nearest neighbors but also with next nearest neighbors (because  $\sigma/2$  is greater than the bond length), and this causes a failure of the simple additive volume approximation. Finally, it is worthwhile to remark that the TraPPE-UA model has already been demonstrated to yield the correct incremental molar volumes of methyl and methylene groups at standard conditions (approximately  $\Delta V_{CH_3} = 34$  mL/mol,  $\Delta V_{CH_2} = 16$  mL/mol);<sup>42</sup> that is, while  $\sigma_{CH_2}$  is larger than  $\sigma_{CH_3}$ , its molar volume increment is much smaller.

**TABLE 4: Liquid Densities at Standard Conditions for the TraPPE-UA Force Field**

alkane	TraPPE-UA $\rho_{\text{liq, std}}$ [g/mL]	exptl $\rho_{\text{liq, std}}$ [g/mL]
2,3-dimethylbutane	0.663 <sub>2</sub>	0.662
2,5-dimethylhexane	0.698 <sub>3</sub>	0.694
3,4-dimethylhexane	0.729 <sub>2</sub>	0.720

**TABLE 5: Comparison of the Second Virial Coefficients for Isobutane and Neopentane<sup>a</sup>**

alkane	$T$ [K]	exptl	PRF	TraPPE-UA
isobutane	296.1	-691	-675 <sub>15</sub>	-535 <sub>4</sub>
	394.6	-384	-376 <sub>7</sub>	-292 <sub>5</sub>
	494.0	-243	-236 <sub>7</sub>	-180 <sub>7</sub>
neopentane	296.1	-976	-935 <sub>12</sub>	-705 <sub>3</sub>
	393.1	-568	-518 <sub>4</sub>	-396 <sub>2</sub>
	492.6	-375	-319 <sub>6</sub>	-242 <sub>4</sub>

<sup>a</sup> The experimental data are taken from Strein and coworkers.<sup>43</sup> The unit for the second virial coefficient is mL/mol. Subscripts show the statistical uncertainty of the final digit.

The trend in  $\epsilon$  is easier to rationalize as  $\epsilon$  should be proportional to the square of the individual polarizabilities. If one assumes that most of the alkane polarizability is in the C–H bonds, while the C–C bonds contribute much less, then  $\epsilon$  would be proportional to the square of the number of C–H bonds in a united atom. The relative values of 16:9:4:1:0 are in fair agreement with the TraPPE-UA  $\epsilon$  parameters.

**B. Specific Densities.** The specific densities at standard conditions for 2,3-dimethylbutane, 2,5-dimethylhexane, and 3,4-dimethylhexane computed for the TraPPE-UA force field in the isobaric–isothermal ensemble are listed in Table 4. The calculated liquid density of 2,3-dimethylbutane is in good agreement with experiment, but the liquid densities of the two octane isomers are about 1% higher than experiment.

**C. Second Virial Coefficients and Compressibility Factors.** The second virial coefficients computed with the TraPPE-UA force field for isobutane and neopentane are smaller in magnitude than the experimental values,<sup>43</sup> as shown in Table 5. This is what we expect for a force field parameterized to reproduce condensed phase properties, as the three-body effects are implicitly taken into account in the two-body force field. Thus, when we look at a strictly two-body property (such as the second virial coefficient), we underestimate the attractive terms as the three-body effect<sup>44</sup> is, on average, repulsive.<sup>45</sup>

Conversely, a force field parameterized to reproduce a two-body property will generally yield parameters which are too attractive for simulations of condensed phases. This is exactly what we observe for the PRF force field (and others have observed for the NERD force field<sup>6</sup>), as the agreement with the second virial coefficient is quite good, while the critical temperatures are too high.

The compressibility factors were computed for each temperature and at the critical point, as listed in ref 40 and Table 3. The TraPPE-UA results generally agree with experiment to within the error bars but overall are too high.

**D. Chain Conformations.** We performed single-molecule simulations to compare the Boltzmann rejection CBMC method used in a previous work, and the coupled–decoupled CBMC method presented in this paper, with a nonbiased determination of the bond bending and torsional angle distributions. The bending and torsional angle distributions were computed for *n*-pentane at 300 K, and Figures 6 and 7 show that all three methods give identical results. This demonstrates that the Boltzmann rejection method is perfectly adequate for linear alkanes. However, Figure 8 shows that the Boltzmann rejection

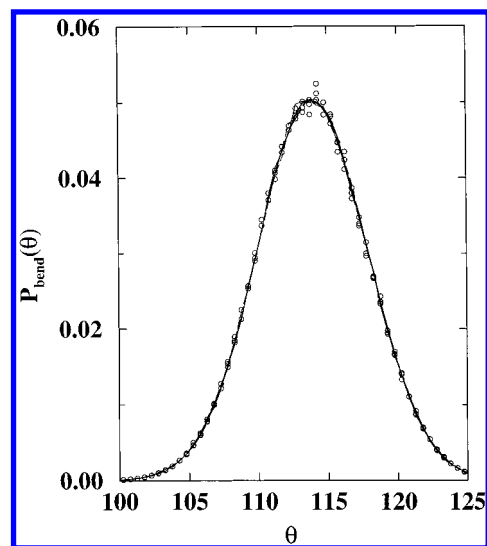


**Figure 6.** Probability distributions for the three bond bending angles in *n*-pentane at 300 K. The observed distributions are shown for the Boltzmann rejection CBMC method (solid line), the coupled–decoupled CBMC method (long dashed line), and the hit-and-miss sampling scheme (open circles).

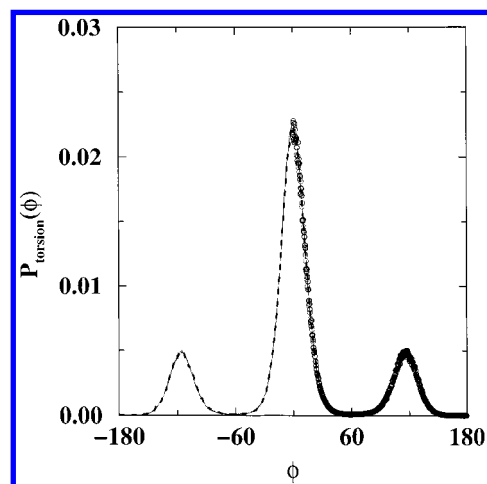


**Figure 7.** Probability distributions for the two torsional angles in *n*-pentane at 300 K. The observed distributions are shown for the Boltzmann rejection CBMC method (thin solid line), the coupled–decoupled CBMC method (thick dashed line), and the hit-and-miss sampling scheme (open circles). For clarity, results for the hit-and-miss scheme are only shown for positive torsional angles.

scheme fails for 3,4-dimethylhexane, as two torsions which should be identical due to the symmetry of the molecule have significantly different distributions at 200 K. This disparity occurs because we label the united atoms in the molecule in order to keep track of them during the simulation. The main chain is labeled 1–2–3–4–5–6, 7 is bonded to 3, and 8 is bonded to 4. The CBMC growth of a molecule in our implementation of the Boltzmann rejection scheme<sup>7</sup> follows a different, predetermined growth pattern depending on which “end” of the molecule the growth originates from. In one direction (starting from 1), the main chain is always grown before the methyl branches, while the opposite is true in the other direction (starting from 6).<sup>7</sup> Thus, one obtains a higher trans fraction for the torsion angle 1–2–3–4 than for 6–5–4–3. The coupled–decoupled CBMC method does not suffer from this problem, and the expected symmetry of torsional angle distributions is obtained. The torsional distributions of 3,4-dimethylhexane for the hit-or-miss method are not shown

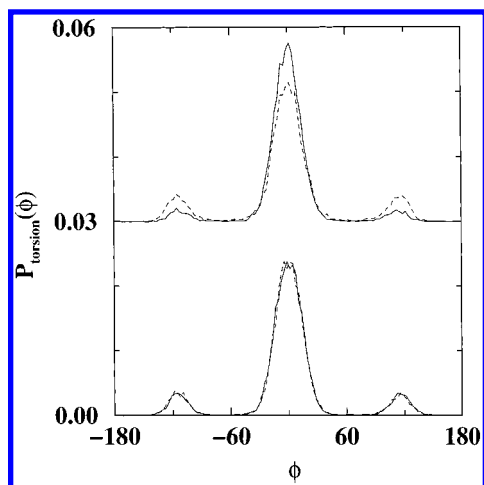


**Figure 8.** Probability distributions for the two (CH<sub>3</sub>)–(CH<sub>2</sub>)–(CH)–(CH) torsional angles in 3,4-dimethylhexane at 200 K. The 1–2–3–4 (solid line) and 6–5–4–3 (dashed line) torsional angles are shown. For clarity, the observed distribution for the Boltzmann rejection CBMC method is displaced by 0.03 compared to the coupled–decoupled CBMC method.

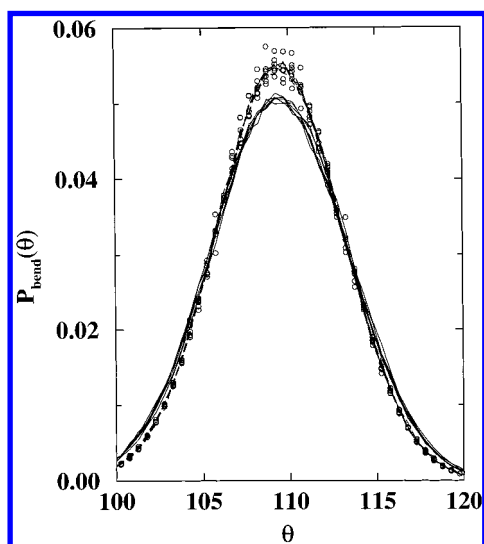


**Figure 9.** Probability distributions for each of the six bond bending angles (identical by symmetry) in neopentane at 300 K. The observed distributions are shown for the Boltzmann rejection CBMC method (solid line), the coupled–decoupled CBMC method (long dashed line), and the hit-and-miss sampling scheme (open circles).

because we could not achieve adequate sampling for this size molecule.

Vlugt and co-workers<sup>26</sup> recently pointed out that there is a problem with generating bond angles via a sequential Boltzmann rejection scheme, and this is illustrated in Figure 9, which shows the bond angle distribution for neopentane at 300 K. Bond angles generated via the Boltzmann rejection method have a wider distribution than those computed from the hit-and-miss sampling method. This occurs because only the final site generated in a sequential Boltzmann rejection feels the entire bond bending potential, while those generated earlier in the growth sequence experience a less restrictive potential. For example, start the growth with the quaternary carbon and then add one site at a time. The second methyl group added only feels one bond bending potential, while the final site added feels three bond bending potentials. This causes those sites generated earlier to have a more broad distribution of bond angles, and this effect is not remedied by randomly choosing the order in which sites are generated, because all of the sites, except the last one,

**TABLE 6.** Torsion Angle Probability Distributions for 2,5-Dimethylhexane and 3,4-Dimethylhexane at 440 K<sup>a</sup>

alkane	bond	$P_g^+$	$P_g^-$	$P_t$
2,5-dimethylhexane	1–2–3–4 <sup>a</sup>	0.293	0.290	0.417
	3–4–5–6 <sup>a</sup>	0.295	0.291	0.414
	7–2–3–4 <sup>a</sup>	0.293	0.291	0.416
	3–4–5–8 <sup>a</sup>	0.293	0.295	0.412
	2–3–4–5	0.033	0.032	0.935
3,4-dimethylhexane	1–2–3–4 <sup>z</sup>	0.124	0.127	0.749
	3–4–5–6 <sup>z</sup>	0.123	0.128	0.749
	1–2–3–7 <sup>y</sup>	0.420	0.421	0.159
	6–5–4–8 <sup>y</sup>	0.424	0.417	0.159
	2–3–4–8 <sup>w</sup>	0.325	0.322	0.353
	5–4–3–7 <sup>w</sup>	0.324	0.325	0.351
	2–3–4–5	0.280	0.285	0.435
	7–3–4–8	0.351	0.348	0.302

<sup>a</sup> Torsional angles are listed by the united-atoms which describe the angle, where the main-chain carbons are numbered 1 through 6 and the methyl branches are 7 and 8. Torsions that are identical due to symmetry are shown with the same letter superscript.

will have a distribution that is too broad. The coupled–decoupled CBMC method produces bond angle distributions in agreement with the nonbiased integration results.

The conformational statistics were analyzed for 2,5-dimethylhexane and 3,4-dimethylhexane in order to determine why these molecules, which have the same composition of united atoms, have different vapor–liquid coexistence curves. The fractions of gauche plus, gauche minus, and trans conformations were computed for each torsional angle at 440 K. The liquid and vapor phases were found to have indistinguishable conformational statistics, so only the liquid phase results are listed in Table 6. Torsional angles which are identical due to the symmetry of the molecule should have the same fraction of trans and gauche angles, and this is the case for the new CBMC algorithm. Notice that the central torsional angle (2–3–4–5) is trans in over 93% of the 2,5-dimethylhexane molecules, while it is trans in less than half of the conformations of 3,4-dimethylhexane. The additional flexibility of 3,4-dimethylhexane allows more freedom to find lower energy intermolecular arrangements than in the case of the much more rigid 2,5-dimethylhexane. This leads to liquid phases which can pack more efficiently to lower the potential energy and therefore increase the heat of vaporization and the critical temperature.

## 5. Concluding Remarks

An extension to the configurational-bias Monte Carlo method is presented which avoids the problems for branched molecules inherent in the traditional Boltzmann rejection scheme. Calculations with this coupled–decoupled CBMC method in the Gibbs ensemble were used to determine the vapor–liquid coexistence curves of branched alkanes for the PRF and TraPPE force fields. For branched alkanes, the PRF force field<sup>5</sup> gives good agreement with second virial coefficients, but predicts critical temperatures that are higher than experiment, while the TraPPE-UA force field produces good critical temperatures but second virial coefficients that are too small in magnitude. The TraPPE-UA force field gives good agreement with the vapor–liquid coexistence curves for small branched alkanes, but the predicted critical temperatures are slightly too high for larger branched alkanes. There was no noticeable difference in the conformations of branched alkanes in the liquid and vapor phases, and it is suggested that the disparity in the trans/gauche ratio of the central torsional angle of 3,4-dimethylhexane and 2,5-dimethylhexane is responsible for the difference in saturated liquid densities and critical temperatures.



**Acknowledgment.** We acknowledge many stimulating discussions with Michael Macedonia, Edward Maginn, Thijs Vlugt, and Berend Smit. Financial support from the National Science Foundation (Grant CTS-9813601), through a Camille and Henry Dreyfus New Faculty Award, a McKnight Land-Grant Professorship, and an Alfred P. Sloan Research Fellowship is gratefully acknowledged. M.G.M. thanks the Department of Energy for a Computational Science Graduate Fellowship. Part of the computer resources were provided by the Minnesota Supercomputing Institute through the University of Minnesota–IBM Shared Research Project and NSF Grant CDA-9502979.

**Supporting Information Available:** Table S1 containing the numerical values of the saturated vapor pressures and coexistence densities for all simulations. This material is available free of charge via the Internet at <http://pubs.acs.org>.

## Appendix: Details of the Coupled–Decoupled CBMC Growth

We generate conformations in a CBMC growth by coupling the Lennard-Jones and torsional selections while splitting the bond bending into several decoupled selections. The procedure we use for performing a regrowth is as follows. Select a molecule of the desired type at random according to a fixed probability. Select an interaction site ( $q$ ) on that molecule at random, and add this to a list of sites that require a growth step. If this is a CBMC molecule exchange move or if a random number uniform on  $(0,1)$  is less than  $p_{\text{all}}$ , then we need to grow every pseudo-atom in the molecule, and we proceed in all directions from  $q$ . Otherwise, we select one pseudo-atom ( $r$ ) bonded to  $q$  in whose direction we will not regrow, while we regrow in all of the other directions emanating from  $q$ . Thus, for the first growth step we will either regrow all, or all except one, of the neighboring sites, while in subsequent steps we regrow all neighboring pseudo-atoms except the one that has already been regrown. The growth proceeds by choosing a pseudo-atom at random from the list of those which require a growth step and regrowing its neighbors according to the algorithm described below. After a growth step is completed, the number of pseudo-atoms ( $t$ ) bonded to each pseudo-atom that was just regrown is computed, and if  $t > 1$  then that pseudo-atom is added to the list of those which require a growth step. This process is repeated until there are no remaining pseudo-atoms which require a growth step. Note that, while this growth order is generated randomly each time we wish to perform a CBMC move, both the old and the new configurations for a particular CBMC attempt must follow the same growth path.

The probability of generating and accepting configurations is given in eqs A1–A7.

$$P_{\text{gen}} = \prod_{n=1}^{n_{\text{step}}} \left[ \frac{\exp(-\beta u_{\text{LJ}}(i)) W_{\text{T}}(i)}{W_{\text{L}}(n)} \right] \left[ \frac{\exp(-\beta u_{\text{tors}}(j))}{W_{\text{T}}(i)} \right] B(n) \quad (\text{A1})$$

$$B(n) = \left( \prod_{a=st(n)}^{n_{\text{grow}}(n)} \left[ \frac{\exp(-\beta u_{\text{bend}}^{[a]}(k))}{W_{\text{P}}^{[a]}(n)} \right] \right) \times \left( \prod_{b=st(n)+1}^{n_{\text{grow}}(n)} \left[ \frac{\exp(-\beta u_{\text{bend}}^{[b]}(k))}{W_{\text{P}}^{[b]}(n)} \right] \right) \quad (\text{A2})$$

$$W_{\text{L}}(n) = \sum_{i=1}^{n_{\text{chLJ}}} \exp(-\beta u_{\text{LJ}}(i)) W_{\text{T}}(i) \quad (\text{A3})$$

$$W_{\text{T}}(i) = \sum_{j=1}^{n_{\text{chtor}}} \exp(-\beta u_{\text{tors}}(j)) \quad (\text{A4})$$

$$W_{\text{P}}^{[x]}(n) = \sum_{i=1}^{n_{\text{chbend}}} \exp(-\beta u_{\text{bend}}^{[x]}(k)) \quad (\text{A5})$$

$$W_{\text{B}}(n) = \left( \prod_{a=st(n)}^{n_{\text{grow}}(n)} W_{\text{P}}^{[a]}(n) \right) \left( \prod_{b=st(n)+1}^{n_{\text{grow}}(n)} W_{\text{P}}^{[b]}(n) \right) \quad (\text{A6})$$

$$P_{\text{acc}} = \text{Min} \left[ 1, \frac{\prod_{n=1}^{n_{\text{step}}} W_{\text{L}}(n)_{\text{new}} W_{\text{B}}(n)_{\text{new}}}{\prod_{n=1}^{n_{\text{step}}} W_{\text{L}}(n)_{\text{old}} W_{\text{B}}(n)_{\text{old}}} \right] \quad (\text{A7})$$

Each growth step ( $n$ ) consists of the following procedure. If this is the first growth step ( $n = 1$ ) and we are regrowing all of the neighboring sites, then choose one of those sites at random, designate it as the “previous” site, and set  $st(n) = 2$ . Otherwise, the one neighboring site which we are not regrowing this step is labeled the “previous” site and  $st(n) = 1$ . Let  $n_{\text{grow}}(n)$  be the number of sites bonded to the current growth site which need to be grown this step. Let  $f$  be the site that we are growing from during this step, and let  $p$  be the “previous” site. For each  $a = st(n)$  to  $n_{\text{grow}}(n)$  determine the  $a$ – $f$ – $p$  angle via a decoupled biased selection based only on  $u_{\text{bend}}$  of the  $a$ – $f$ – $p$  angle (denoted  $u_{\text{bend}}^{[a]}$ ), and compute the Rosenbluth weight  $W_{\text{P}}^{[a]}(n)$ . The selection of trial angles for this step is made uniformly on the cosine of the angle in order to properly account for the phase space term. Once all of the  $a$ – $f$ – $p$  angles have been selected, then the  $b$ – $f$ – $c$  angles are determined for each  $b = st(n) + 1$  to  $n_{\text{grow}}(n)$  via a biased, decoupled selection based on the energy

$$u_{\text{bend}}^{[b]} = \sum_{c=st(n)}^{b-1} u_{\text{bend}}(b-f-c) \quad (\text{A8})$$

This is done by choosing the dihedral angle between  $b$ – $f$ – $p$  and  $st(n)$ – $f$ – $p$  uniformly on  $(0, 2\pi)$   $n_{\text{chbend}}$  times, computing the  $b$ – $f$ – $c$  angles, and selecting one trial in a biased fashion based upon  $u_{\text{bend}}^{[b]}$ .

Once all of the bond bending angles have been determined, we perform  $n_{\text{chLJ}}$  biased selections based upon all of the torsional angles that contain  $f$  and  $p$  along the central bond, except in the special case where  $p$  is one of the sites that is being grown this step. For each of the  $n_{\text{chLJ}}$  selections,  $n_{\text{chtor}}$  random orientations for site  $st(n)$  on a cone with axis  $f$ – $p$  are chosen uniformly on  $(0, 2\pi)$ , and the torsional energy for all of the beads grown this step is computed and used to select one torsional angle in a biased fashion. This is the first step of the coupled biased selection of the torsional and nonbonded energy terms. The second step is to compute the nonbonded interaction energy for each of the  $n_{\text{chLJ}}$  orientations that were chosen during the torsional selections, and choose one site in a coupled biased fashion based upon  $u_{\text{LJ}}$  and the torsional Rosenbluth weights.

If this is the special case where  $p$  is one of the sites that is grown this step, then there are no existing torsional angles at this step of the growth process. In that case, a decoupled biased

selection is made based solely upon the nonbonded interaction energies for  $n_{\text{chLJ}}$  random orientations of both  $p$  and the rest of the sites grown this step. This is equivalent to performing a coupled biased selection that has identical Rosenbluth weights for all  $n_{\text{chLJ}}$  torsional angles.

We briefly explored the CBMC growth parameter space and found that values of  $n_{\text{chLJ}} = 8$ ,  $n_{\text{chtor}} = 100$ , and  $n_{\text{chbend}} = 1000$  yield good acceptance rates without being excessively expensive.

## References and Notes

- (1) Williams, D. E. *J. Chem. Phys.* **1967**, *47*, 4680.
- (2) Ryckaert, J. P.; Bellemans, A. *Faraday Discuss. Chem. Soc.* **1978**, *66*, 95.
- (3) Toxvaerd, S. J. *J. Chem. Phys.* **1990**, *93*, 4290.
- (4) Martin, M. G.; Siepmann, J. I. *J. Phys. Chem. B* **1998**, *102*, 2569.
- (5) Poncela, A.; Rubio, A. M.; Freire, J. J. *Mol. Phys.* **1997**, *91*, 189.
- (6) Nath, S. K.; Escobedo, F. A.; de Pablo, J. J. *J. Chem. Phys.* **1998**, *108*, 9905.
- (7) Siepmann, J. I.; Martin, M. G.; Mundy, C. J.; Klein, M. L. *Mol. Phys.* **1997**, *90*, 687.
- (8) Zhuravlev, N. D.; Siepmann, J. I. *Fluid Phase Equilib.* **1997**, *134*, 55.
- (9) Vlugt, T. J. H.; Martin, M. G.; Smit, B.; Siepmann, J. I.; Krishna, R. *Mol. Phys.* **1998**, *94*, 727.
- (10) Cui, S. T.; Cummings, P. T.; Cochran, H. D. *Fluid Phase Equilib.* **1997**, *141*, 45.
- (11) Lorentz, H. A. *Ann. Phys.* **1881**, *12*, 127.
- (12) Berthelot, D. C. *R. Hebd. Séances Acad. Sci.* **1898**, *126*, 1703.
- (13) van der Ploeg, P.; Berendsen, H. J. C. *J. Chem. Phys.* **1982**, *94*, 3271.
- (14) Jorgensen, W. L.; Madura, J. D.; Swenson, C. J. *J. Am. Chem. Soc.* **1984**, *106*, 813.
- (15) Mundy, C. J.; Balasubramanian, S.; Bagchi, K.; Siepmann, J. I.; Klein, M. L. *Faraday Discuss.* **1996**, *104*, 17.
- (16) Mooij, G. C. A. M.; Frenkel, D.; Smit, B. *J. Phys.: Condens. Matter* **1992**, *4*, L255.
- (17) Laso, M.; de Pablo, J. J.; Suter, U. W. *J. Chem. Phys.* **1992**, *97*, 2817.
- (18) Panagiotopoulos, A. Z. *Mol. Phys.* **1987**, *61*, 813.
- (19) Panagiotopoulos, A. Z.; Quirke, N.; Stapleton, M.; Tildesley, D. J. *Mol. Phys.* **1988**, *63*, 527.
- (20) Smit, B.; de Smedt, P.; Frenkel, D. *Mol. Phys.* **1989**, *68*, 931.
- (21) Siepmann, J. I. *Mol. Phys.* **1990**, *70*, 1145.
- (22) Siepmann, J. I.; Frenkel, D. *Mol. Phys.* **1992**, *75*, 59.
- (23) Frenkel, D.; Mooij, G. C. A. M.; Smit, B. *J. Phys.: Condens. Matter* **1992**, *4*, 3053.
- (24) de Pablo, J. J.; Laso, M.; Suter, U. W. *J. Chem. Phys.* **1992**, *96*, 2395.
- (25) Dijkstra, M. *J. Chem. Phys.* **1997**, *107*, 3277.
- (26) Vlugt, T. J. H.; Krishna, R.; Smit, B. *J. Chem. Phys.* **1999**, *1102*.
- (27) Macedonia, M. D.; Maginn, E. J. *Mol. Phys.*, submitted.
- (28) Tuckerman, M. E.; Berne, B. J.; Martyna, G. J. *J. Chem. Phys.* **1992**, *97*, 1990.
- (29) Esselink, K.; Loyens, L. D. J. C.; Smit, B. *Phys. Rev. E* **1995**, *51*, 1560.
- (30) Mackie, A. D.; Tavittian, B.; Boutin, A.; Fuchs, A. H. *Mol. Simul.* **1997**, *19*, 1.
- (31) Rowlinson, J. S.; Widom, B. *Molecular Theory of Capillarity*; Oxford University Press: New York, 1989; p 261.
- (32) Rowlinson, J. S.; Swinton, F. L. *Liquids and Liquid Mixtures*, 3rd ed.; Butterworth: London, 1982; pp 70–75.
- (33) Atkins, P. W. *Physical Chemistry*, 4th ed.; W.H. Freeman and Company: New York, 1990; Chapter 6.
- (34) Allen, M. P.; Tildesley, D. J. *Computer Simulation of Liquids*; Oxford University Press: Oxford, 1987.
- (35) McDonald, I. R. *Mol. Phys.* **1972**, *23*, 41.
- (36) McQuarrie, D. A. *Statistical Mechanics*; Harper and Row: New York, 1976; Chapter 12.
- (37) Lal, M.; Spencer, D. J. *Chem. Soc., Faraday Trans. 2* **1973**, *69*, 1502.
- (38) Cheney, W.; Kincaid, D. *Numerical Mathematics and Computing*, 3rd ed.; Brooks/Cole: Pacific Grove, 1994; Chapter 5.
- (39) Errington, J. R.; Panagiotopoulos, A. Z. *J. Chem. Phys.* **1998**, *109*, 1093.
- (40) The numerical values of the saturated vapor pressures and coexistence densities for all simulations are listed in the Supporting Information (Table S1).
- (41) Smith, B. D.; Srivastava, R. *Thermodynamic Data for Pure Compounds: Part A Hydrocarbons and Ketones*; Elsevier: Amsterdam, 1986.
- (42) Martin, M. G.; Zhuravlev, N. D.; Chen, B.; Carr, P. W.; Siepmann, J. I. *J. Phys. Chem. B*, in press.
- (43) Strein, V. K.; Lichtenthaler, R. N.; Schramm, B.; Schafer, K.; *Ber. Bunsen-Ges. Phys. Chem.* **1971**, *75*, 1308.
- (44) Axilrod, B. M.; Teller, E. *J. Chem. Phys.* **1943**, *11*, 299.
- (45) Stenschke, H. *J. Chem. Phys.* **1994**, *100*, 4705.